CrystEngComm

Robust and Well-controlled TiO2-Al2O3 Binary Nano-array Rooted Ceramic Honeycomb for Efficient Propane Combustion

Journal:	*CrystEngComm*
Manuscript ID	CE-ART-11-2018-002012.R1
Article Type:	Paper
Date Submitted by the Author:	08-Feb-2019

Complete List of Authors:	Xiong, Juxia; Huazhong Normal University Luo, Zhu; Huazhong Normal University Yang, Ji; Huazhong Normal University Guo, yanbing Guo; Central China Normal University School of Chemistry, Institute of Environmental and Applied Chemistry Adimali , Piyadasa; University of Connecticut, b. Department of Materials Science and Engineering & Institute of Materials Science Wang, Sibo; University of Connecticut, Institute of Materials Science Son, Hoang; University of Connecticut, b. Department of Materials Science and Engineering & Institute of Materials Science Fang, Yarong; Huazhong Normal University Hu, Siyu; Huazhong Normal University Yang, Weiwei; Chinese Academy of Sciences, Research Center for Eco-Environmental Sciences Deng, Hongtao; Central China Normal University, Key Laboratory of Pesticide and Chemical Biology Zhang, Lizhi; Central China Normal University, Gao, Pu-Xian; University of Connecticut,

Journal Name

ARTICLE

Robust and Well-controlled TiO_2-Al_2O_3 Binary Nanoarray Rooted Ceramic Honeycomb for Efficient Propane Combustion

Received 00th January 20xx,
Accepted 00th January 20xx

DOI: 10.1039/x0xx00000x

www.rsc.org/

Juxia Xiong[a], Zhu Luo[a], Ji Yang[a], Yanbing Guo*[a], Adimali Piyadasa[b], Sibo Wang[b], Son Hoang[b], Yarong Fang[a], Siyu Hu[a], Weiwei Yang[a], Hongtao Deng[a], Lizhi Zhang[a], Pu-Xian Gao*[b]

The catalytic total oxidation of short chain alkane released from automobile exhaust is still a big challenge in Volatile organic compounds (VOCs) elimination. The significant degradation of catalytic activity after hydrothermal aging is a widely existed issue. Herein, we report a facile one-pot hydrothermal method to successfully grow TiO_2-Al_2O_3 binary nanoarray onto the 3D channel surfaces of ceramic honeycombs. Such a binary nanoarray is heterogeneously rooted on the cordierite honeycomb channel surface with intimately separated nanowire arrays of anatase-TiO_2 and mesoporous γ-Al_2O_3, which exhibits excellent robustness under mechanical vibration, thermal, and hydrothermal aging. Moreover, the Pt/TiO_2-Al_2O_3 binary nanoarray catalyst for propane conversion reaches rapidly to 80 % at temperature as low as 224 ℃, suggesting the binary nanoarray catalyst a promising candidate for practical application.

1. Introduction

As the fossil fuel consumption tremendously increases with the increasing number of stationary and mobile sources deployed globally, the energy and environmental sustainability becomes a great challenge in recent decades.[1-3] The pollutants released from fuel combustion, mainly composed of unburned hydrocarbons (HCs), nitrogen oxides species (NO_x), particulate matter and so on, have great drawbacks to environment and human health.[4] Among the exhaust components, HCs contribute a great portion to the overall volatile organic compounds (VOCs) in the atmosphere, which has been proved to not only lead to serious health effect but also promote the formation of photochemical smog.[5-7] To mitigate the environment issue associated with HCs release, high-efficient after-treatment strategies are desired urgently.[8-13] Catalytic oxidation of HCs, in which HCs are completely oxidized into CO_2 and H_2O at a relatively lower temperature with the assistant of efficient catalysts, is one of the most effective methods to eliminate HCs. However, comparing with the unsaturated hydrocarbons, the catalytic total oxidation of alkane (especially short chain alkane such as methane, propane) released from automobile exhaust is still a big challenge due to the stable molecular structure and strong C-H bond.[14]

Monolithic catalysts have been widely applied in stationary and mobile source VOCs treatment system because of their outstanding emission reduction efficiency and low pressure drop.[4,15] Recently, the nanoarray monolithic catalysts with well-controlled structure, composition, morphology, and porosity, show great potential as a next-generation alternative for current washcoated monolithic catalysts. A broad spectrum of individual, core-shell and multicomponent metal oxide nanoarray have been fabricated and demonstrated with promising catalytic activity for propane total oxidation as well as excellent materials utilization efficiency.[16,17] However, the significant degradation of catalytic activity after hydrothermal aging prevent its further application in practical after treatment system.[7,13]

Among composite nanomaterials, binary nanoarray which has two kinds of individual nanoarray with well controlled space between each component, has been fabricated on planar substrate. It serves as model catalysts and show unique photocatalytic property, which could be ascribed to the intimate interaction between dissimilar sub-components.[18] The unique, well-controlled space between each nanoarray component may be able to enhance hydrothermal stability by effectively preventing the crystal growth that is induced by sintering effect at high temperature. So far, however, binary nanoarray based monolithic catalysts with excellent catalytic activity and hydrothermal stability has not been achieved.

Herein, we explored a facile and cost-effective hydrothermal synthesis process for large-scale growth of crystalline TiO_2-Al_2O_3 binary nanoarray on the channel walls of 3D honeycomb monoliths. The morphologies and structures of TiO_2-Al_2O_3 binary nanoarray could be well tuned by the hydrothermal temperature and reaction time. In addition, a group of stability tests including thermal, hydrothermal stability and mechanical

[a] Key Laboratory of Pesticide & Chemical Biology of Ministry of Education, Institute of Environmental and Applied Chemistry, College of Chemistry, Central China Normal University, Wuhan 430079, People's Republic of China;.
[b] Department of Materials Science and Engineering & Institute of Materials Science, University of Connecticut, Storrs, CT 06269-3136, USA;.
*E-mail: guoyanbing@mail.ccnu.edu.cn; puxian.gao@uconn.edu
†Electronic Supplementary Information (ESI) available: [details of any supplementary information available should be included here]. See DOI: 10.1039/x0xx00000x

stability, demonstrated its excellent robustness in long term application. Pt loaded TiO_2-Al_2O_3 binary nanoarray monolithic catalysts displayed an excellent low-temperature activity and remarkable hydrothermal stability for propane combustion. The propane conversion efficiency reached rapidly to 80 % at temperature as low as 224 ℃, once the propane oxidation light-off around 200 ℃. In this study, the TiO_2-Al_2O_3 binary nanoarray integrated 3D honeycomb monoliths could be used as functional devices in energy and environmental applications including catalytic combustion reactor, catalyst supports, and particulate matter filers.

2. Experimental Section

2.1 Synthesis of Catalysts

2.1.1 Material and methods

All chemicals used in this investigation are purchased from Sigma-Aldrich, Inc. The reagents are of analytical grade and used directly without further purification. Cordierite monolith substrates are purchased from Corning, Inc. and Shandong Aofu Environmental Technology Co., Ltd.

2.1.2 Synthesis of TiO_2-Al_2O_3 binary nanoarray

The composite mesoporous TiO_2-Al_2O_3 binary nanoarray grown on the 3D walls of honeycomb monolith was prepared via one step solvothermal synthesis. Cordierite ($2MgO•2Al_2O_3•5SiO_2$) honeycomb monoliths (400 cells/in.^{2}, 0.15 mm average wall thickness) were used as substrates. A piece of ceramic cordierite honeycomb substrate (1.3 cm×1.3 cm×1.0 cm) was ultra-sonicated for 10 min in sequential in different solvents including deionized water (50 mL), acetone (50 mL), normal hexane (30 mL), and ethanol (50 mL). Then the substrate was dried in air stream at 70 ℃. In the synthesis process, the treated honeycomb cordierite was put into a 28 mL teflon-lined stainless steel autoclave containing a mixture solution of 10 mL toluene (C_7H_8), 1 mL tetrabutyl titanate, 1 mL titanium tetrachloride ($TiCl_4$) (1 M in toluene), and 1 mL hydrochloric acid (HCl) (37 wt%). [19] The reaction system was heated up to certain temperature (200 ℃ or 240 ℃) using an oven in air, and maintained for 24 h. Then, the sample was taken out of the autoclave and rinsed in DI water, acetone, and ethanol in sequence for three times to remove loose powder precipitated on the surface of the monolith walls. Finally, after drying in air at 70 ℃ for 3 h, the obtained sample was placed into the muffle furnace, annealed at 800 ℃ in air for 10 h. The obtained sample was named as TiO_2-Al_2O_3 binary nanoarray.

2.1.3 Preparation of Pt/TiO_2-Al_2O_3 binary nanoarray catalysts

Pt was loaded on TiO_2-Al_2O_3 binary nanoarray via two different methods: sequential colloidal deposition and wet impregnation. For sequential colloidal deposition method, TiO_2-Al_2O_3 sample was firstly annealed under 10 % H_2/Ar flow at 500 ℃ for 1 h. The sample was taken out and sonicated in DI water for 2 h. A certain amount of Pt (0.5 mg) colloidal in ethylene glycol solution was diluted by 3 mL acetone in a vial to prepare total loading of 0.3 wt% Pt/ TiO_2-Al_2O_3 substrate. The substrate was immersed in the solution and sonicated for 2 h until the solution color changed from blackish to transparent (indication of Pt absorption on to monolith). The vial was then left in fume hood until all acetone vaporized. Finally, the substrate was heated up in the oven for 10 h at 110 ℃. The obtained sample was named as Pt/TiO_2-Al_2O_3 (C) binary nanoarray. For impregnation method, the TiO_2-Al_2O_3 sample was cleaned by sonicating in DI water for 10 times, 30 mins for each time to wash out all Cl-ions. A solution of tetraammineplatinum (II) nitrate was prepared by dissolving the amount of tetraammineplatinum (II) nitrate calculated as 0.3 % Pt loading (TiO_2-Al_2O_3 substrate) in 2.5 mL of DI water. The sample was immersed in this solution and sonicated for 5 minutes, then taken out and dried in oven (110 ℃) for 20 min. The dip-coating process was repeated with 10 times until the remaining tetraammineplatinum (II) nitrate solution was 1.5 mL. The substrate was then heated up to 110 ℃. The solution was injected to the substrate using a pipette. The injection process was repeated until all the Pt solution was used up. The substrate was heated up in oven at 110 ℃ for 4 h and annealed at 500 ℃ for 1 h. The obtained sample was named as Pt/TiO_2-Al_2O_3 (I) binary nanoarray.

2.2 Characterization

The XRD spectrum was obtained from 10 ° to 90 ° at a scan rate of 0.2°/scan over a Rigaku D/Max-2200 X-ray diffractometer (XRD) with Cu-K_α (40 kV, 40 mA) radiation. Field emission scanning electron microscope (FESEM, JSM-7600F, JEOL Inc., Japan) equipped with energy dispersive X-ray spectrometer (EDS) was employed to analyze the morphology and element distribution of the as-prepared samples. The structure of the synthesized samples was analyzed using high resolution transmission electron microscopy (HR-TEM, JEM-2010, JEOL Inc., Japan). A Micromeritics ASAP2020M were measured at 77 K to the surface areas and pore size distribution of the samples. Before the tests, the corresponding samples were degassed at 150 °C for 6 h to remove physically adsorbed impurities.

2.3 Stability Tests

The thermal, hydrothermal, and mechanical stability of TiO_2-Al_2O_3 binary nanoarray were investigated in this study. The mechanical stability was examined under pulse high velocity airflow (0 to 50 L/min, 30 s/cycles) for 200 cycles. The TiO_2-Al_2O_3 binary nanoarrays monolithic catalysts were also sonicated in water for 30 min in a Branson 3210 Ultrasonic Cleaner with 40 kHz frequency to further evaluate its mechanical adhesion between nanoarray and ceramic substrates. The variation of BET surface area was monitored every 24 hours during the 800 ℃, 72 h annealing process. The hydrothermal stability of TiO_2-Al_2O_3 binary nanoarray was investigated at 800 ℃ for 10 h with 10 % De-ionized water vapor.

2.4 Catalytic Performance Evaluation

The Pt/TiO_2-Al_2O_3 catalytic oxidation activity was tested by using propane as a probe molecule. The experiments were conducted in a fixed-bed quartz reactor (1.5 cm of internal diameter). Before the test, the catalysts and quartz wool (to avoid the axial diffusion) were placed in the reactor. The sample was firstly purged with N_2 at 100 ℃ for 30 minutes. During the test, the inlet gas was composed of 0.92 % propane and 8 % oxygen balanced by nitrogen with a flow rate of 150 mL/min. The size of Pt/TiO_2-Al_2O_3 binary nanoarray monolithic catalysts used for the performance test was 5 mm×5 mm×10 mm. The space velocity was 36,000 h^{-1}. The catalytic performance data was recorded from 100 ℃ to 600 ℃.

3. Results and discussion

3.1 Morphology and Structure of TiO_2-Al_2O_3 Binary Nanoarray

As shown in Figure 1a, the TiO_2-Al_2O_3 binary nanoarray coated cordierite monolith shows white colour with no-obvious colour change compared to bare cordierite monolith. A further morphology investigation under SEM (Figure 1b-f) suggests that the highly aligned nanoarray with needle-like shape was densely and uniformly grown on the channel wall of monolith substrate. The length of needle-like nanowire was approximately 3-5 μm and the thickness was about 200-400 nm, showing a perpendicularly aligned structure (Figure 1c) on the substrate. The EDS mapping collected at the cross section of nanoarray sample (Figure 1d), indicates that the longer nanowire arrays grown on the substrate are mainly composed of aluminum, while the shorter nanowires close to the bottom of monolith substrate are composed of titanium. The densely packed short nanorod array (about 2 μm in length and 100 nm in thickness) on the bottom could be clearly observed under SEM at higher magnification in Figure 1e. The top-view SEM image reveals that the long Al composed nanowires grew out of the substrate and formed bundles of flower type structure (Figure 1f). Transmission electron microscope (TEM) was used for further characterizing the structure of TiO_2-Al_2O_3 binary nanoarray. As shown in Figure 2a, the mesoporous nanowires, about 3-4 μm in length and 200 nm in diameter, are observed. Higher magnification TEM image (Figure 2b) illustrates that those porous structures around 6 nm wide interconnected with each other to form a highly porous morphology. The unique mesoporous structure is beneficial for the preparation of high performance supported catalysts.[18,20-23] From the high resolution transmission electron microscope (HRTEM) image (Figure 2c), the lattice spacing of plane is approximately 2.39 nm, which can be indexed to the (311) plane of gamma Al_2O_3 (γ-Al_2O_3) (JCPDS no. 29-0063). The powder XRD profiles of TiO_2-Al_2O_3 binary nanoarray is shown in Figure 2d. The diffraction pattern shows intense and sharp characteristic peaks at 25.3, 48.1, 62.7, 68.8, 75.1, and 82.2 corresponding to the (101), (200), (204), (116), (215), and (303) planes in anatase phase TiO_2 (JCPDS no. 88-1175 and JCPDS no. 84-1286).

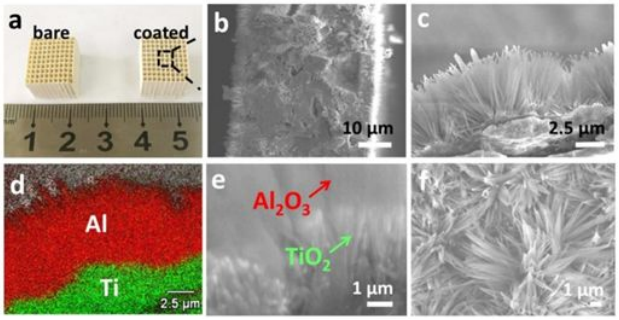

Figure 1. Typical morphology and structure of TiO_2-Al_2O_3 binary nanoarray on monolith. (a) photograph of bare ceramics (left) and TiO_2-Al_2O_3 binary nanoarray coated monolith (right). Scanning Electronic Microscopy (SEM) images: (b) low magnification view of cordierite monolithic channel wall grown with TiO_2-Al_2O_3 binary nanoarray. (c) Cross-sectional view of TiO_2-Al_2O_3 binary nanoarray on monolithic channel wall. (d) EDS Ti and Al element mapping of nanoarray in Figure 1c. (e) Higher magnification view of Al_2O_3 nanoarray (top) and TiO_2 nanoarray (bottom). (f) Top view of TiO_2-Al_2O_3 binary nanoarray on cordierite monolith.

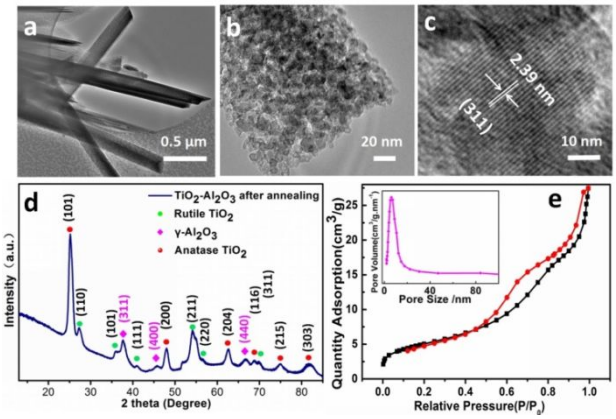

Figure 2. Transmission Electron Microscope (TEM) images of Al_2O_3 nanoarray at different magnifications: (a) a bundle of mesoporous nanowires, (b) high magnification view of a typical single nanowire, (c) High Resolution Transmission Electron Microscope (HRTEM) image of Al_2O_3 mesoporous nanowire; (d) XRD pattern of the TiO_2-Al_2O_3 binary nanoarray; (e) N_2 adsorption/desorption isotherm of the TiO_2-Al_2O_3 binary nanoarray, inset: the BJH pore size distribution of TiO_2-Al_2O_3 binary nanoarray.

XRD diffraction peaks at 27.4, 36.1, 41.2, 54.3, 56.6, and 72.4 correspond to the (110), (101), (111), (211), (220), and (311) planes in rutile phase TiO_2 (JCPDS no. 75-1751), respectively. While, the characteristic peaks at 37.6°, 45.8°, and 66.7° could be attributed to the γ-Al_2O_3 nanostructures, which correspond to the (311), (400), and (440) planes of the cubic crystal structure of γ-Al_2O_3 (JCPDS no. 29-0063). No obvious diffraction peaks of other phases (δ-, θ-, α-phase) are observed, indicating the other possible phase of Al_2O_3 are completely transformed to crystalline γ-Al_2O_3 after 800 ℃ annealing.[24] According to the XRD analysis, the nanowires could be attributed to the gamma

Al_2O_3, which is consistent with TEM analysis (Figure 2c). The nitrogen adsorption-desorption isotherm of the TiO_2-Al_2O_3 material (Figure 2e) is consistent with IUPAC type IV with distinct hysteresis loops, indicating the existence of mesoporous structure. The BET specific surface area of mesoporous TiO_2-Al_2O_3 binary nanoarray integrated monolith is about 23 m^2g^{-1}. The inset of Figure 2e shows the BJH pore size distribution of as-prepared TiO_2-Al_2O_3 nanoarray, which is ranged from 5 to 20 nm. The pore size distribution mainly concentrates at 4.2 nm, and such porosity could be attributed to the decomposition of $Al(OH)_3$.[25] The result is consistent with TEM results and further confirms the existence of mesoporous structure. As mentioned above, the large specific surface area and narrow mesopore size distribution could effectively increase the dispersion of supported active phase and the amount of catalytic active sites, which will result in higher catalytic performance.[26]

3.2 Stability test of TiO_2-Al_2O_3 binary nanoarray

Excellent mechanical stability and thermal stability are essential for monolithic catalysts since the inevitable mechanical vibration and extreme high temperature conditions in various practical industrial applications including automotive and stationary emission control. To evaluate the mechanical stability of as-prepared TiO_2-Al_2O_3 binary nanoarray, the higher velocity pulse air flow was firstly applied to the ceramic device. As shown in Figure 3, the air flow is circulated in "on" and "off" mode (50 L/min, 0 L/min) for 200 cycles. The SEM images before and after the air flow flush (Figure 3b, c) shows that the nanoarray retained unexceptionable array structures after the pulse high velocity air flow treatment, which displays that the TiO_2-Al_2O_3 binary nanoarray own excellent mechanical stability. To further evaluate the robustness of the monolith catalysts, ultrasound sonication with frequency of 40 kHz and power of 250 W was applied to the TiO_2-Al_2O_3 binary nanoarray monolithic substrate immersed in DI water. The nanoarray also reserves its ordered structures very well throughout the 30 min sonication in water. As shown in Figure 3d, after 5 min sonication, no obvious weight loss is examined. When prolonging the sonication time to 15 min, the weight of TiO_2-Al_2O_3 binary nanoarray decreased slightly to 98.1 % of its original weight. When the sonication time extended to 30 min, the weight of TiO_2-Al_2O_3 binary nanoarray based monolithic catalyst further decreased to 95.0 %. As indicated from the inset SEM images in Figure 3d, there are no obvious morphology changes throughout the entire monolith substrate even after 30 min sonication. The weight loss may be attributed to the removal of precipitated TiO_2-Al_2O_3 powder on the monolith channel surface during the synthesis process. The well retained nanoarray morphology and slight weight loss demonstrate that the robust TiO_2-Al_2O_3 binary nanoarray has remarkable mechanical stability and hold great potential for practical industrial application. With the inevitable presence of water vapor in combustion exhaust emissions. Hydrothermal stability

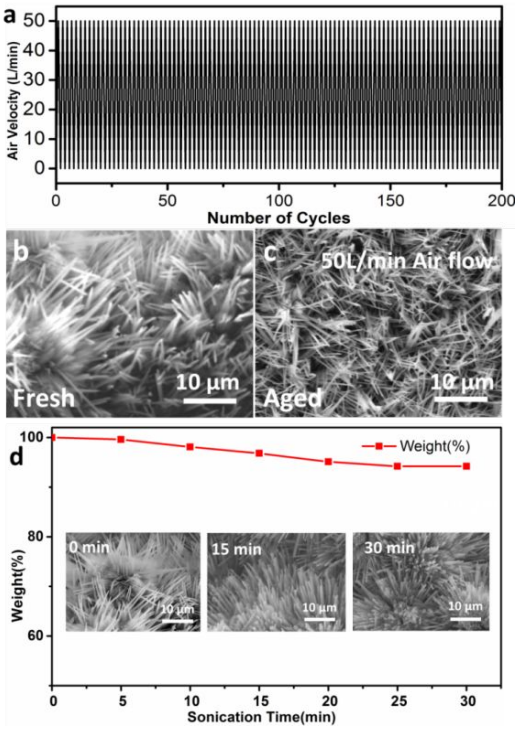

Figure 3. Pulsatile flow flushing, ultrasonic vibration testing, and corresponding SEM images before and after testing: (a) plot of pulse air flushing test (air velocity vs. circles); the TiO_2-Al_2O_3 binary nanoarray before (b) and after (c) the pulsatile flow flushing; (d) plot of sonication time dependent weight loss of TiO_2-Al_2O_3 binary nanoarray (weight vs. sonication time); inset images in (d): the SEM images of the TiO_2-Al_2O_3 binary nanoarray after sonication for 0 min, 15 min, and 30 min.

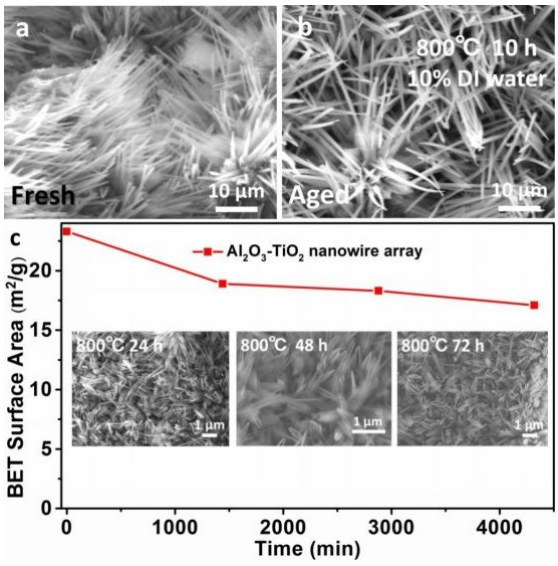

Figure 4. SEM images of TiO_2-Al_2O_3 binary nanoarray obtained before (a) and after 10 % DI water vapor, 800 ℃, 10 h hydrothermal aging (b); (c) time dependent BET surface area variation and morphology change (inset in c) at 800 ℃, 72 h thermal aging in air.

of TiO_2-Al_2O_3 binary nanoarray coated monolith substrates is another key aspect need to be evaluated. The morphology variation before and after 800 ℃ isothermal aging in 10 % water steam was investigated by SEM. As shown in Figure 4a-b, the nanoarray is densely packed and uniformly coated on the substrates (Figure 4b) after hydrothermal aging, exhibiting no observable morphology change comparing with the fresh sample (Figure 4a). The result reveals the TiO_2-Al_2O_3 binary nanoarray has good hydrothermal stability under extreme conditions. Moreover, in Figure 4c, the variation of BET surface area during isothermal annealing process was investigated. The BET surface area has a relatively large decline in the first 1400 min (about 24 h), which decreases from 23.1 m^2/g to 18.8 m^2/g. After that, the plot of the surface area remains gradually smooth and steady till the end of 72 h annealing process. The inserted SEM images display that there is no obvious morphology change of the nanoarray structure at low magnification after thermal aging for 72 h at 800 ℃. The BET surface area loss (about 3 m^2/g for the sample) during the first 24 h may mainly be attributed to high temperature sintering leaded small crystal grain growth and aggregation.[27] The phase transition from brookite/anatase to rutile among a small portion of TiO_2 nanoarray may also affect the surface area decrease.[28] In addition, the high temperature isothermal annealing test with and without steam reveals that the as-prepared TiO_2-Al_2O_3 binary nanoarray has an excellent thermal and hydrothermal stability.

3.3 Morphology Evolution and Growth Mechanism of TiO_2-Al_2O_3 Binary Nanoarray

To unfold the growth mechanism and ensure the successful large-scale manufacturing of the nanoarray based honeycomb monoliths, it is crucial to investigate the structural and morphological evolution of the TiO_2-Al_2O_3 binary nanoarray with the solvothermal temperature and reaction time. Therefore, we systematically investigated the morphology evolution of nanoarray grew on honeycomb monolith under different hydrothermal temperatures (160 ℃, 200 ℃, 240 ℃) and reaction time (12 h, 24 h), as shown in Figure 5, respectively.

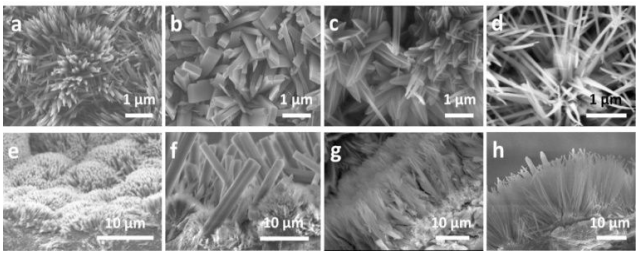

Figure 5. Top-view and cross-section view SEM images of nanoarray grown on the cordierite substrate with different reaction time and solvothermal temperature at: (a, e) 160 ℃, 12 h; (b, f) 200 ℃, 12 h; (c, g) 240 ℃, 12 h; (d, h) 240 ℃, 24 h.

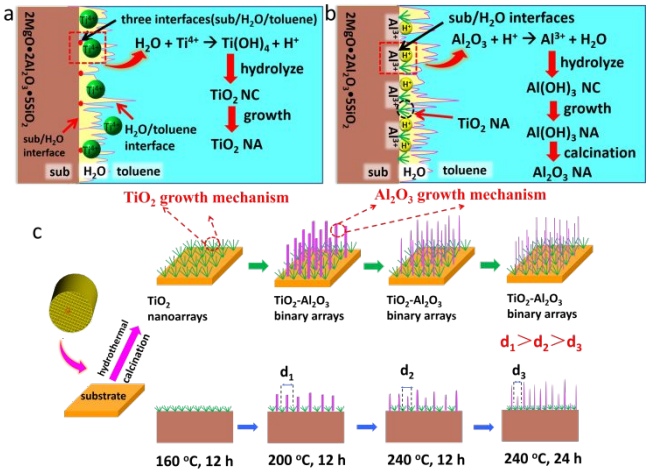

Scheme 1. Schematic illustration of TiO_2-Al_2O_3 binary nanoarray growth mechanism: (a) The TiO_2 nanoarray grown at 160 ℃; (b) the TiO_2-Al_2O_3 binary nanoarray grown at temperature above 200 ℃ (200 ℃, 240 ℃); (c) the schematic morphology of TiO_2-Al_2O_3 binary nanoarray synthesized at different solvothermal temperature (160 ℃, 200 ℃, 240 ℃) and reaction time (12h, 24h). The diameter and length of TiO_2 nanorod and Al_2O_3 nanowire is denoted as D (TiO_2), D (Al_2O_3) and L (TiO_2), L (Al_2O_3). The space between the TiO_2 nanowires was donated as "d_1", "d_2", "d_3" for samples grown at 200 ℃/12 h, 200 ℃/24 h, and 240 ℃/24 h, respectively. NC: Nanocrystalline; NA: Nanoarray. The brown color represents substrate; The white color represents water; The blue-green color represents toluene.

The SEM images exhibit that the nanoarray grows uniformly on the substrate at different temperatures (Figure 5a-h). The flower-shaped TiO_2 nanowires are observed after hydrothermal growing at 160 ℃ for 12 h (Figure 5a, e). The length of nanoarray is 3-5 μm and the thickness is 200-300 nm. With the hydrothermal temperature increasing to 200 ℃ (Figure 5b, f), the Al_2O_3 rod-like arrays with average length of 8-10 μm and the thickness of 600-800 nm grew all over the honeycomb substrates. More compelling, the cross-section SEM image (Figure 5f) clearly displays the hierarchical nanoarray structure on honeycomb substrate: beneath the longer Al_2O_3 micro-rod arrays, there are densely packed layers of TiO_2 wire-like nanoarrays. The results reveal that the temperature increased to 200 ℃, the TiO_2-Al_2O_3 binary nanoarray grows uniformly on the substrate forming hierarchical nanoarray structure. With the solvothermal temperature rising further to 240 ℃, the Al_2O_3 rod-like nanoarray starts to form sheet-like nanoarray. The length of nanoarray is 10-12 μm and the thickness is 300-400 nm in Figure 5c, g. When the reaction time prolonged to 24 h at 240 ℃, the nanosheet then starts to form needle-like nanowire. The length of nanoarray is 12-14 μm and the thickness is 100-200 nm. Compared with the nanoarray grown for 12 h, the nanowires are more dense and uniform, as shown in Figure 5d, h. It may be due to TiO_2 crystal splitting is induced with the reaction time prolonging, thus leading to the fast TiO_2 crystal growth.[34] In addition, the formation of the first TiO_2 nanoarray layers can change surface energy and enhance surface stability, thus promoting the further grain growth of Al_2O_3 nanoarray.[29]

Therefore, the thickness of Al_2O_3 nanoarray became thinner, and the length of Al_2O_3 nanoarray becomes longer. The phenomenon reveals that the size and shape of Al_2O_3 nanoarray can be tuned by the solvothermal temperature.

Based on the above results, the growth mechanism is proposed in Scheme 1. In the nanoarray synthesis, the tetrabutyl titanate and titanium tetrachloride were used as the precursor and dissolved into the nonpolar solvent toluene. Hydrochloric acid is crucial for preventing hydrolysis of the precursor and ensuring a stable pH. The small polar water contained in the HCl solution is alien to the nonpolar toluene. With the increasing solvothermal temperature, water with lower system energy will diffuse away from the high-energy water/toluene and form emulsion. Ti precursors (Ti^{4+}) are gradually hydrolyzed by water on the water/toluene interfaces and formed TiO_2 nucleus either homogeneously in the water/toluene interface or heterogeneously in the water/toluene/substrate.[19] As displayed in Scheme 1a, at a lower temperature of 160 ℃，due to the hydrophilic property of inserted cordierite monolith wall, the three phase interface of water/toluene/cordierite will form on the cordierite wall surface with water closely contacting with cordierite due to its wettability. Ti^{4+} precursors will be hydrolyzed by water at the water/toluene/cordierite interfaces, thus resulting in formation of the first TiO_2 nanocrystalline on the substrate. Then TiO_2 nanocrystalline (TiO_2 NC) built up via crystal growth right after the nucleation.[30] Subsequently, the TiO_2 nanowire (TiO_2 NW) array forms on the honeycomb substrate as the result of oriented crystal growth. When the temperature increased to a higher temperature of 200 ℃ (as shown in Scheme 1b), as a result of Al_2O_3 surface/H_2O interactions, the dissolution of the alumina oxide may be induced by adsorption of H^+ ions.[31,32] The surface Al_2O_3 in ceramic cordierite ($2MgO•2Al_2O_3•5SiO_2$) substrates between the gap of flower shaped TiO_2 nanowire bundle will be etched and dissolve into HCl solution due to high acidity of precursor solution. Then the dissolved Al^{3+} can be hydrolyzed by water and form $Al(OH)_3$ nanocrystalline ($Al(OH)_3$ NC) layer. With continuous hydrolysis and subsequent crystallization, the $Al(OH)_3$ nanorods will grow between the gaps of TiO_2 nanoarray bundles on the substrates. Finally, the sample was calcined at 800 ℃ under air for 10 h. The mesoporous Al_2O_3 nanowires are fabricated from the decomposition of $Al(OH)_3$, in which the mesopores on Al_2O_3 nanowire may be generated due to the evaporation of water vapor. According to the XRD and TEM results (Figure 2), the synthesized Al_2O_3 is gamma phase alumina. That is because that the transformation temperature of γ-Al_2O_3 phases is in the range of 500-850 ℃.[33,34] During the sintering process of 800 ℃ in air for 10 h, even though the dehydration reactions ($2Al(OH)_3 \rightarrow \gamma\text{-}Al_2O_3 + 3H_2O$) played a fundamental role in the formation of γ-Al_2O_3, it may be also accompanied with the transformation of γ-Al_2O_3 from other Al_2O_3 phases. The formation of TiO_2 nanoarray can change a surface energy and enhance a surface stability, thus promoting the further grain growth of Al_2O_3 nanoarray.[29,35] It may also account for the gradually increased length of Al_2O_3 nanoarray with the rising of solvothermal temperature. As the solvothermal temperature further increased to 240 ℃, the TiO_2-Al_2O_3 still retains its binary hierarchical structure with the boom layer TiO_2 nanoarray grows more uniformly and densely all over the substrate (Figure 5 and Scheme 1a, 1c). But the morphology of Al_2O_3 nanorod has changed greatly. The diameter of Al_2O_3 nanorod reduces significantly from 800 nm to about 300 nm, with the morphology evolving from Al_2O_3 nanorod arrays into wire-shaped Al_2O_3 nanowire arrays. This phenomenon infers that the space between the TiO_2 nanowire becomes narrower with the increasing temperature, which may be due to the fast TiO_2 nucleation and crystal growth. As the result of fast nucleation and growth, the TiO_2 nanowire density increases and the gap between TiO_2 nanowire bundles decreases ($d_1 > d_2 > d_3$). The narrower poky space then lead to the conversion of rod-like Al_2O_3 nanoarray into aligned Al_2O_3 nanowire clusters. Therefore, the Al_2O_3 nanowires grow thinner and longer at 240 ℃ than that of 200 ℃.

3.4 Catalytic Performance

To demonstrate the application of TiO_2-Al_2O_3 binary nanostructures and develop highly efficient catalysts for hydrocarbon emission control, Pt were loaded on TiO_2-Al_2O_3 binary nanoarray integrated monolith with a weight ratio of 0.3 wt% via two different loading methods. In colloidal method, the well-defined Pt nanoparticles are dispersed into acetone to form a colloidal solution and loaded onto TiO_2-Al_2O_3 binary nanoarray through a dip-coating process (denoted as Pt/TiO_2-Al_2O_3 (C)). While in the wet impregnation method, Pt precursor is dissolved into DI water to form a solution and loaded onto

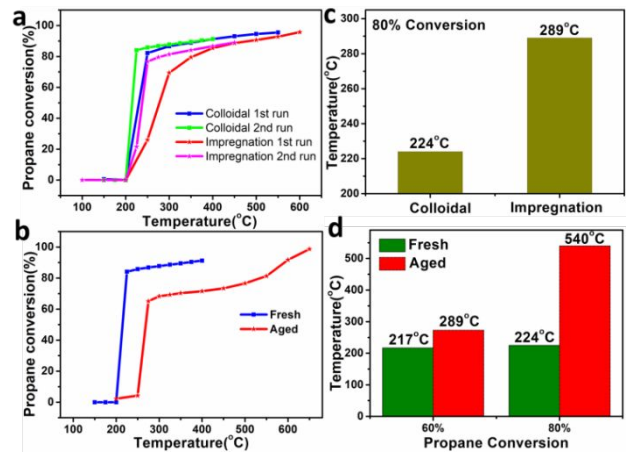

Figure 6. (a) Propane oxidation performance of Pt-loaded TiO_2-Al_2O_3 catalysts with colloidal and wet impregnation method; (b) 80 % conversion temperature of propane over Pt/TiO_2-Al_2O_3 catalyst with colloidal and impregnation method, respectively; (c) light-off curve of fresh and aged sample prepared with sequential colloidal deposition method; (d) 60 % and 80 % conversion temperature of Pt/TiO_2-Al_2O_3 (C) catalyst as fresh and aged at 800 ℃ over the course of 10 h on 10 % water stream, respectively.

TiO_2-Al_2O_3 binary nanoarrays through a dip-coating and post-annealing process (denoted as Pt/ TiO_2-Al_2O_3 (I)). The propane oxidation is selected as a probe reaction, and the activity measurements as a function of temperature are carried out from 100 ℃ to 600 ℃. The light-off curves of propane oxidation over as-synthesized Pt/TiO_2-Al_2O_3 catalysts are depicted in Figure 6a. It can be found that both of the Pt/TiO_2-Al_2O_3 catalysts start to show catalytic activity at temperatures above 200 ℃. And for both Pt/TiO_2-Al_2O_3 (C) and Pt/TiO_2-Al_2O_3(I) catalysts, the second test cycle (2nd run) always shows better catalytic activity (TC_{80}=224 ℃ , TI_{80}=289 ℃) than 1st run (TC_{80}=249 ℃ , TI_{80}=354 ℃), which may be attributed to the decomposition of organic ligand or other contaminant on Pt surface after the 1st run. While, the Pt/ TiO_2-Al_2O_3 (C) shows better catalytic activity than Pt/TiO_2-Al_2O_3 (I), which may be likely due to the better Pt nanoparticle size distribution and particle dispersion on Pt/TiO_2-Al_2O_3 (C) catalysts. For instance, the catalytic activity of Pt/Al_2O_3, Pt/CeO_2, and Pt/TiO_2 catalyst (Pt loading was about 0.5 wt% for all the samples) achieved 60 % conversion for propane (T_{60}) at 417 ℃, 342 ℃, 337 ℃, respectively.[36] While in our work, the fresh Pt/TiO_2-Al_2O_3 (C) catalyst achieves 60 % propane conversion at 217 ℃, which is about 200 ℃, 125 ℃, and 120 ℃ lower than the literature reported Pt/Al_2O_3, Pt/CeO_2, Pt/TiO_2 catalysts. Typically, T_{60} of Pt/Al_2O_3 is in the range from 350 ℃ to 420 ℃, and addition of active solid oxide additives as co-catalysts could further improve the low temperature performance of Pt catalysts. It is observed that the addition of vanadium and tungsten to Pt/Al_2O_3 increased the catalytic hydrocarbon oxidation activity. The T_{60} of the best performed Pt/V_2O_5/Al_2O_3 (0.4 % Pt loading) catalysts and Pt/WO_x/Al_2O_3 (1 % Pt loading) catalysts were 280 ℃and 258 ℃, respectively.[37] Vanadium oxide and tungsten oxide loaded on Pt/Al_2O_3 were the key factors affecting Pt dispersion, Pt oxidation state, and reactivity of Pt sites.[38-40] It is worth noting that our Pt/TiO_2-Al_2O_3 binary nanoarray monolithic catalysts show about 63 ℃ and 41 ℃ lower T_{60} comparing with Pt/V_2O_5/Al_2O_3 and Pt/WO_x/Al_2O_3. It is clear that the Pt/TiO_2-Al_2O_3 binary nanoarrays catalyst exhibits excellent propane oxidation activity, which is probably due to that the binary nanoarray can bring a highly uniform distribution of Pt species within the nanowires.[41,42] To better understand the catalytic stability, the effect of hydrothermal aging on catalytic activity over Pt/TiO_2-Al_2O_3 catalysts is also studied. Here, we select the Pt/TiO_2-Al_2O_3 (C) catalyst as a model platform to investigate the catalytic activity dependence on hydrothermal aging. The high-temperature aging was carried out at 800 ℃ with continuous calcining for 10 h in flowing air with 10 % steam. The propane oxidation light-off curves of fresh and aged catalysts (Figure 6c) display that the aged catalyst has a lower propane oxidation activity than fresh catalyst. Figure 6d shows 60 %, 80 % propane conversion temperatures of the aged Pt/TiO_2-Al_2O_3 (C) catalyst, which is delayed from 217 ℃ to 289 ℃ (72 ℃) and 224 ℃ to 540 ℃ (316 ℃), respectively. It is reasonable to deduce that high temperature sintering can cause the small precious metal grains to aggregate and merge into bigger particles. As a result, the surface area decreases, thus causing catalytic activity degradation. [43]

In general, the activity of Pt-supported catalysts decreases significantly after high-temperature aging in an oxidative atmosphere. [44,45] It was reported that T_{60} of the best performed 1 wt% Pt/Al_2O_3 powder catalyst, after aging at 800 ℃ with 5 % saturated steam for even only 2 h, raised (around 50 ℃) from 350 ℃ to 400 ℃, compared with the fresh catalysts.[46] For our Pt/TiO_2-Al_2O_3 (C) binary nanoarray catalyst, even though hydrothermal aging at 800 ℃ with 10 % saturated steam for 10 h, the Pt/TiO_2-Al_2O_3 (C) catalyst still exhibit much better catalytic activity comparing with the Pt/Al_2O_3 power catalysts. It indicates that the Pt/TiO_2-Al_2O_3 (C) catalyst has good hydrothermal stability, which may be due to the nanoarray structure and the strong metal-support interaction on Pt/TiO_2 interface.[47] Further structure and formulation optimization will improve the catalytic activity and stability with no doubt.

In summary, the Pt/TiO_2-Al_2O_3 (C) exhibits superior catalytic performance, compared with the Pt/TiO_2-Al_2O_3 (I). The Pt/TiO_2-Al_2O_3 (C) catalyst achieves as high as 80 % at a relatively low temperature of 224 ℃ for the propane oxidation, which is much better than the traditional noble metal powder catalyst. The fresh Pt/TiO_2-Al_2O_3 (C) with a faster reaction tendency reaches 60 % propane conversion at much lower temperatures (217 ℃) than the aged Pt/TiO_2-Al_2O_3 (C) (289 ℃). It also indicates that the Pt/TiO_2-Al_2O_3 (C) catalyst has good hydrothermal stability even after hydrothermal aging at 800 ℃ with 10 % saturated steam for 10 h. The binary TiO_2-Al_2O_3 of different morphologies in nanostructured catalysts could be as a model platform to practically investigate the catalytic activity dependence on the nanostructure size and shape, which may hold crucial importance in the tunability of catalytic activity for better heterogenous catalyst design.

Conclusions

In conclusion, hierarchical TiO_2-Al_2O_3 binary nanoarray has been uniformly grown on the inner walls of 3D honeycomb by a facile one-pot hydrothermal method, and the morphology can be effectively tuned by hydrothermal temperatures and reaction times. The as-prepared TiO_2-Al_2O_3 binary nanoarray exhibits excellent robustness through a thorough mechanical, thermal, and hydrothermal stability test, which will reduce the catalysts layer erosion and improve the lifespan of the monolithic catalysts. The Pt/TiO_2-Al_2O_3 (C) catalysts display excellent catalytic performance for propane oxidation with 80 % conversion at 224 ℃. Moreover, the Pt/TiO_2-Al_2O_3 (C) aged under 800 ℃ with 10 % saturated steam for 10 h still reaches 60 % propane conversion at 289 ℃, which is much better than the traditional noble metal powder catalyst. The as-fabricated TiO_2-Al_2O_3 binary nanoarray may open up promising application of the automotive exhaust emission, electronics, catalysis, and biomedical research. And the novel binary nanoarray structure and fabrication strategy demonstrated here will provide a new and effective strategy for the rational design of low cost, scalable and high-performance structured catalysts.

Acknowledgements

The authors are grateful for the financial support from the National Natural Science Foundation of China (No. 21777051). The Recruitment Program of Global Young Experts start-up funds, National Engineering Laboratory for Mobile Source Emission Control Technology (NELMS2017A11), The Program of Introducing Talents of Discipline to Universities of China (111 program, B17019), and the US DOE/National Energy Technology Laboratory (Award number: DE-EE0000210).

References

1. S. Pan, J. Li, O. Noonan, X. Fang, G. Wan, C. Yu and L. Wang, *Environ. Sci. Technol.*, 2017, **51**, 5098-5107.
2. E. M. Sunderland, C. T. Driscoll, Jr., J. K. Hammitt, P. Grandjean, J. S. Evans, J. D. Blum, C. Y. Chen, D. C. Evers, D. A. Jaffe, R. P. Mason, S. Goho and W. Jacobs, *Environ. Sci. Technol.*, 2016, **50**, 2117-2120.
3. S. Zhao and J. Li, *ChemCatChem*, 2015, **7**, 1966-1974.
4. C. Jiang, Y. T. Hsieh, H. Zhao, H. Zhou and Y. Yang, *J. Am. Chem. Soc.*, 2015, **137**, 11069-11075.
5. S. I. Suárez-Vázquez, S. Gil, J. M. García-Vargas, A. Cruz-López and A. Giroir-Fendler, *Appl. Catal. B: Environ.*, 2018, **223**, 201-208.
6. Z. Ye, J. M. Giraudon, N. Nuns, P. Simon, N. De Geyter, R. Morent and J. F. Lamonier, *Appl. Catal. B: Environ.*, 2018, **223**, 154-166.
7. S. Xie, Y. Liu, J. Deng, S. Zang, Z. Zhang, H. Arandiyan, and H. Dai, Environ. Sci. Technol. 2017, **51**, 2271−2279.
8. X. Hu, J. H. Belle, X. Meng, A. Wildani, L. A. Waller, M. J. Strickland and Y. Liu, *Environ. Sci. Technol.*, 2017, **51**, 6936-6944.
9. T. Wang, D. C. Quiros, A. Thiruvengadam, S. Pradhan, S. Hu, T. Huai, E. S. Lee and Y. Zhu, *Environ. Sci. Technol.*, 2017, **51**, 6990-6998.
10. A. G. Rappold, J. Reyes, G. Pouliot, W. E. Cascio and D. Diaz-Sanchez, *Environ. Sci. Technol.*, 2017, **51**, 6674-6682.
11. V. Franco, T. Zacharopoulou, J. Hammer, H. Schmidt, P. Mock, M. Weiss and Z. Samaras, *Environ. Sci. Technol.*, 2016, **50**, 13151-13159.
12. P. Karjalainen, L. Ntziachristos, T. Murtonen, H. Wihersaari, P. Simonen, F. Myllari, N. O. Nylund, J. Keskinen and T. Ronkko, *Environ. Sci. Technol.*, 2016, **50**, 12504-12511.
13. D. Pi, W. Li, Q. Lin, Q. Huang, H. Hu, and C. Shao, Energy Technol. 2016, **4**, 943–949.
14. Z. Hu, Z. Wang, Y. Guo, L. Wang, Y. Guo, J. Zhang and W. Zhan, *Environ. Sci. Technol.*, 2018, **52**, 9531-9541.
15. Y. Guo, G. Liu, Z. Ren, A. Piyadasa and P.-X. Gao, *CrystEngComm*, 2013, **15**, 8345-8352.
16. Z. Ren, Y. Guo, Z. Zhang, C. Liu and P.-X. Gao, *J. Mater. Chem. A*, 2013, **1**, 9897-9906.
17. S. Wang, S. Du, W. Tang, S. Hoang, X. Lu, W. Xiao, B. Zhang, J. Weng, E. Schneer, Y. Guo, J. Ding, Z. Zhang and P.-X. Gao, *ChemCatChem*, 2018, **10**, 2184-2189.
18. L. Wen, R. Xu, Y. Mi and Y. Lei, *Nat. Nanotechnol.*, 2017, **12**, 244-250.
19. A. J. M. Mackus, M. A. Verheijen, N. Leick, A. A. Bol and W. M. M. Kessels, *Chem. Mater.*, 2013, **25**, 1905-1911.
20. X. Tian, L. Li, Y. Hu, H. Zhang, Y. Liu, H. Chen, G. Ding and Z. Zou, *RSC Adv.*, 2013, **3**, 7880-7883.
21. M. M. Shulaker, G. Hills, R. S. Park, R. T. Howe, K. Saraswat, H. P. Wong and S. Mitra, *Nature*, 2017, **547**, 74-78.
22. H. Rao, W. Wu, Y. Liu, Y. Xu, B. Chen, H.Chen, D. Kuang and C. Su, *Nano Energy.,* 2014, **8**, 1-8.
23. D. Gu, W. Schmidt, C. M. Pichler, H. J. Bongard, B. Spliethoff, S. Asahina, Z. Cao, O. Terasaki and F. Schuth, *Angew. Chem. Int. Ed. Engl.*, 2017, **56**, 11222-11225.
24. M. Cheng, S. Duan, H. Fan, X. Su, Y. Cui and R. Wang, *Chem. Eng. J.*, 2017, **327**, 100-108.
25. X. Qian, M. Ren, D. Yue, Y. Zhu, Y. Han, Z. Bian and Y. Zhao, *Appl. Catal. B: Environ.*, 2017, **212**, 1-6.
26. W. Zhang, X. Lin, Y. Sun, D. Bin, A. Cao, and L. Wan, *ACS Appl. Mater. Inter.,* 2015, **7**, 27031−27034.
27. S. Wang, Z. Ren, W. Song, Y. Guo, M. Zhang, S. L. Suib and P.-X. Gao, *Catal. Today*, 2015, **258**, 549-555.
28. B. Solsona, T. García, R. Sanchis, M. D. Soriano, M. Moreno, E. Rodríguez-Castellón, S. Agouram, A. Dejoz and J. M. López Nieto, *Chem. Eng. J.*, 2016, **290**, 273-281.
29. J. Lee, E. J. Jang and J. H. Kwak, *J. Catal.*, 2017, **345**, 135-148.
30. Y.-M. Kim, S.-H. Hong and D.-Y. Kim, *J. Am. Ceram. Soc.*, 2000, **83**, 2809-2812.
31. W. Cai, Y. Hu, J. Chen, G. Zhang and T. Xia, *CrystEngComm*, 2012, **14**, 972-977.
32. G. R. Desiraju, *J. Am. Chem. Soc.*, 2013, **135**, 9952-9967.
33. A. A. S. Gonçalves, M. J. F. Costa, L. Zhang, F. Ciesielczyk and M. Jaroniec, *Chem. Mater.*, 2018, **30**, 436-446.
34. S. Tabesh, F. Davar and M. R. Loghman-Estarki, *J. Alloy. Compd.*, 2018, **730**, 441-449.
35. A. Forgács, K. Moldován, P. Herman, E. Baranyai, I. Fábián, G. Lente and J. Kalmár, *J. Phys. Chem. C,* 2018, **122**, 19161-19170.
36. V.V. Sinels'nikov, N.N. Tolkachev, S.S. Goryashchenko, N.S. Telegina, A.Yu. Stakheev, Kinetics and Catalysis 2006, **47**, 98–105.
37. J. Choi, S. Zhang and J. M. Hill, *Catal. Sci. Technol.*, 2012, **2**, 179-186.
38. M. S. Avila, C. I. Vignatti, C. R. Apesteguía and T. F. Garetto, *Chem. Eng. J.*, 2014, **241**, 52-59.
39. M. S. Avila, C. I. Vignatti, C. R. Apesteguía, V. Venkat Rao, K. Chary and T. F. Garetto, *Catal. Lett.*, 2009, **134**, 118-123.
40. S. L. Bergman, J. Granestrand, Y. Tang, R. S. París, M. Nilsson, F. F. Tao, C. Tang, S. J. Pennycook, L. J. Pettersson and S. L. Bernasek, *Appl. Catal. B: Environ.*, 2018, **220**, 506-511.
41. H. Ge, C. Wang and L. Yin, *J. Mater. Chem. A*, 2015, **3**, 17359-17368.
42. N. Padmanathan, H. Shao, D. McNulty, C. O'Dwyer and K. M. Razeeb, *J. Mater. Chem. A*, 2016, **4**, 4820-4830.
43. J. Wang, J. Wen, and M. Shen, *J. Phys. Chem. C,* 2008, **112**, 5113-5122.
44. S. Yoon, K. Oh, F. Liu, J. H. Seo, G. A. Somorjai, J. H. Lee and K. An, *ACS Catal.*, 2018, **8**, 5391-5398.
45. H. Wang, M. Liu, Y. Ma, K. Gong, W. Liu, R. Ran, D. Weng, X. Wu and S. Liu, *ACS Catal.*, 2018, **8**, 2796-2804.
46. Y. Nagai, T. Hirabayashi, K. Dohmae, N. Takagi, T. Minami, H. Shinjoh and S. Matsumoto, *J. Catal.*, 2006, **242**, 103-109.
47. T. Yeh, S. Linic and P. E. Savage, *ACS Sustain. Chem. Eng.*, 2014, **2**, 2399-2406

Robust and Well-controlled TiO_2-Al_2O_3 Binary Nano-array Rooted Ceramic Honeycomb for Efficient Propane Combustion

Juxia Xiong[a], Zhu Luo[a], Ji Yang[a], Yanbing Guo*[a], Adimali Piyadasa[b], Sibo Wang[b], Son Hoang[b], Yarong Fang[a], Siyu Hu[a], Weiwei Yang[a], Hongtao Deng[a], Lizhi Zhang[a], Pu-Xian Gao*[b]

Controlled fabrication with well-tuned size and shape by temperature and reaction time of TiO_2-Al_2O_3 binary nanoarray successfully grow onto the 3D channel surfaces of ceramic honeycombs, exhibiting excellent robustness and high catalytic performance for propane.